Journal of Magnetic Resonance **140,** 69–83 (1999)
Article ID jmre.1999.1823, available online at http://www.idealibrary.com on IDEAL®

Absolute EPR Spin Echo and Noise Intensities

George A. Rinard, Richard W. Quine, Ruitian Song, Gareth R. Eaton, and Sandra S. Eaton

Department of Engineering and Department of Chemistry and Biochemistry, University of Denver, Denver, Colorado 80208

Received August 27, 1998; revised May 27, 1999

EPR signal and noise, calculated from first principles, are compared with measured values of signal and noise on an S-band (ca. 2.7 GHz) EPR spectrometer for which all relevant gains and losses have been measured. Agreement is within the uncertainty of the calculations and the measurements. The calculational model that provided the good agreement is used to suggest approaches to optimizing spectrometer design. © 1999 Academic Press

Key Words: **EPR; ESR; electron spin echo; absolute signal intensity; signal-to-noise; noise.**

INTRODUCTION

Electron spins could be used to understand many problems in materials sciences and biomedical sciences if the EPR signal were strong enough. A crucial question then is how many spins should one be able to observe? To address this question one needs to calculate absolute signal intensities and compare these with noise for a particular spectrometer configuration. General introductions in texts and monographs express results in terms of the relative signal-to-noise (S/N) ratio. Absolute signal and noise measurements are much more difficult, because one now has to measure all gains and losses and characterize noise that accompanies the signal. The absolute determination of spin concentration has been described as the most difficult measurement one can make with EPR equipment (*1, 2*). Alger (*2*) summarized the state of the art as of 1968, and little has been reported since then. Hyde and co-workers analyzed the signal and noise of a spectrometer for the case in which source microwave power was incident during data collection (e.g., saturation recovery) and considered the relative benefits of cryogenically cooled microwave preamplifiers (*3*). They obtained good agreement between calculated and observed RMS system noise voltages.

This paper reports EPR signal and noise in an S-band time-domain EPR spectrometer and compares the measured values with calculated values. Agreement is within the uncertainties of the comparison. On the basis of these results we outline an approach to designing spectrometers to maximize S/N in time-domain EPR.

DESCRIPTION OF THE S-BAND SPECTROMETER

The S-band (2–4 GHz) EPR spectrometer (Fig. 1) was built on much the same design philosophy as our L-band spectrometer (*4*). Since this spectrometer serves as an engineering station for the development of new spectrometer and resonator concepts, it is constructed with extensive flexibility, and as will be discussed below, better S/N would be obtained if there were fewer devices between the resonator and the detector. However, this extreme flexibility facilitated the comparisons reported here. We list below the properties of the components in the EPR signal path. Some of the specific components may no longer be available commercially, and/or components with better specifications may now be available, but the numerical values for these particular components are crucial to the quantitative analysis presented.

A pair of transfer switches (components 70 and 71—component numbers throughout the text refer to the numbers in Figs. 1 and 2) provide multiple signal paths and facilitate exploration of the properties of spectrometer components and resonators, especially the crossed-loop resonator (*5, 6*). There are many signal amplification options. One path has no microwave amplification in the bridge. Most commonly, this is used in conjunction with an external microwave amplifier, such as the coolable Berkshire amplifier (component 108) in the cryostat assembly as described below (Fig. 2). We have also used it here to compare signal and noise with and without a microwave preamplifier. Also in the bridge there are two paths with microwave amplifiers. These amplifiers (components 34 and 35), made by MITEQ (Hauppauge, New York), have gains of 44.7 and 27.7 dB at the frequency (ca. 2.7 GHz) at which most of our measurements were made. To compare the echo amplitude obtained using the Berkshire amplifier with that obtained using the MITEQ amplifiers, it was necessary to add a coaxial cable to bypass the Berkshire amplifier and then select the path in the bridge that uses one of the MITEQ amplifiers. Although the spectrometer assembly includes a cryostat, and one amplifier is located in the cryostat, unless specified otherwise all measurements reported in this paper were taken at room temperature, which was ca. 294 K.

The resonator used, Fig. 3, is of the loop–gap resonator (LGR) type (*7*) and is conceptually similar to resonators used

1090-7807/99 $30.00

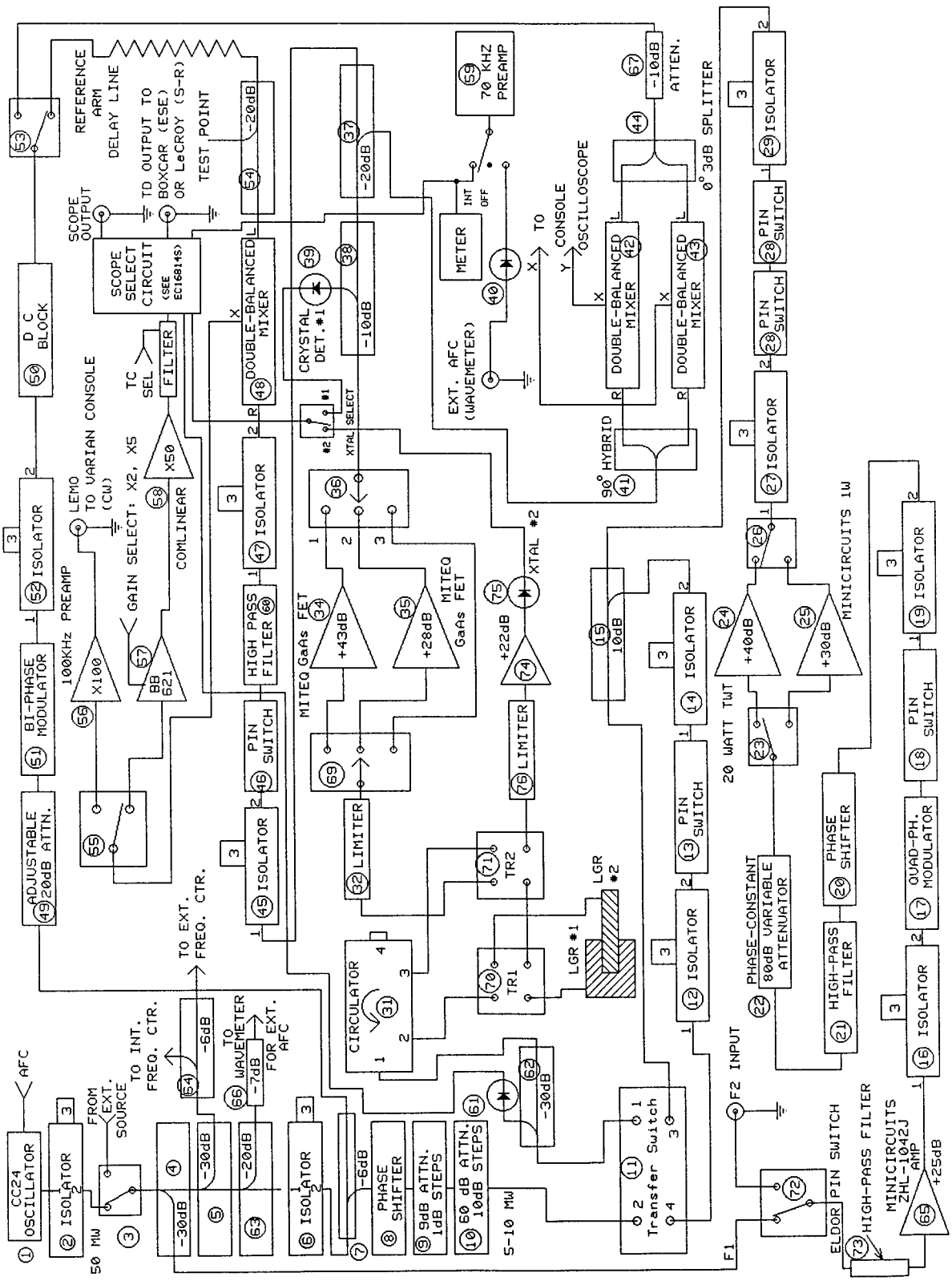
CC24 OSCILLATOR
ISOLATOR
FROM EXT. SOURCE
50 MW
AFC
TO INT. FREQ. CTR.
-6dB
-30dB
-20dB
TO WAVEMETER -7dB FOR EXT. AFC
ISOLATOR
-6dB
PHASE SHIFTER
9dB ATTN. 1dB STEPS
60 dB ATTN. 10dB STEPS
5-10 MW
-30dB
Transfer Switch
F2 INPUT
F1
ELDOR PIN SWITCH
HIGH-PASS FILTER
MINICIRCUITS ZHL-1042J AMP +25dB
ISOLATOR
HIGH-PASS FILTER
PHASE-CONSTANT 80dB VARIABLE ATTENUATOR
PHASE SHIFTER
QUAD-PH. MODULATOR
ISOLATOR
PIN SWITCH
20 WATT TWT
+40dB
+30dB
MINICIRCUITS 1W
ISOLATOR
PIN SWITCH
ISOLATOR
10dB
ISOLATOR
PIN SWITCH
ISOLATOR
TR1
TR2
LGR #1
LGR #2
CIRCULATOR
LIMITER
LIMITER
+22dB
XTAL #2
MITEQ GaAs FET
+43dB
+28dB
MITEQ GaAs FET
XTAL SELECT
#1
#2
CRYSTAL DET.#1
-10dB
-20dB
ADJUSTABLE 20dB ATTN.
BI-PHASE MODULATOR
100KHz PREAMP
X100
LEMO TO VARIAN CONSOLE (CW)
GAIN SELECT: X2, X5
BB 621
COMLINEAR
X50
TC SEL
FILTER
HIGH PASS FILTER
PIN SWITCH
ISOLATOR
DOUBLE-BALANCED MIXER
D C BLOCK
ISOLATOR
SCOPE OUTPUT
SCOPE SELECT CIRCUIT (SEE EC16814S)
TD OUTPUT TO BOXCAR (ESE) OR LeCROY (S-R)
TEST POINT
REFERENCE ARM DELAY LINE
-20dB
-10dB
70 KHZ PREAMP
METER
INT
OFF
EXT. AFC (WAVEMETER)
TO CONSOLE OSCILLOSCOPE
DOUBLE-BALANCED MIXER
DOUBLE-BALANCED MIXER
90° HYBRID
0° 3dB SPLITTER
-10dB ATTEN.
ISOLATOR
PIN SWITCH
ISOLATOR
ISOLATOR
PIN SWITCH
ISOLATOR
TO EXT. FREQ. CTR.

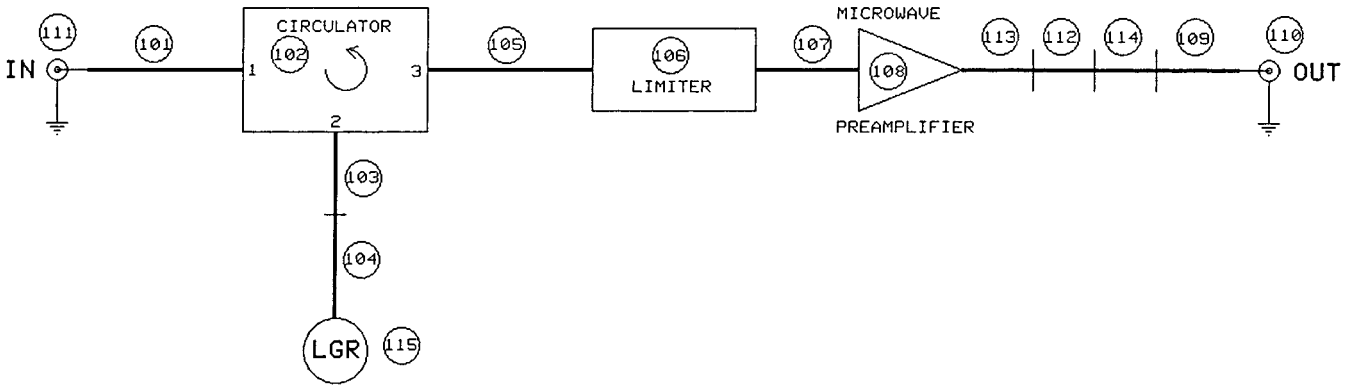

FIG. 2. Schematic diagram for the spectrometer components located in the cryostat rather than in the bridge. All cables are semirigid coax with either solid shield or tinned braided shield, 0.141 inch in diameter. All connectors are sma. The bridge is connected to the cryostat assembly with two flexible coaxial cables with sma connectors. (101) 22.9-cm coax; (102) magnetically shielded circulator (Passive Microwave Technology), positioned approximately parallel to B_0; (103) 20.3-cm coax; (104) 22.9-cm coax built into the resonator; (105) 7.6-cm coax; (106) GaAs diode limiter, 1.4-dB insertion loss; (107) 7.6-cm coax; (108) microwave preamplifier, Berkshire 41.8-dB gain at 2.7 GHz, 50–62 K noise temperature at room temperature, (1.0-dB NF); (109) 30.5-cm coax; (110), (111) sma bulkhead feedthrough; (112) 7.6-cm coax; (113), (114) sma 90° bend; (115) resonator described in Fig. 3. The various coaxial cables and sma adapters were dictated by the geometry of the cryostat and the size of the magnet (e.g., to keep the circulator in as low a magnetic field and as low a temperature (when cooled) as feasible).

in some EPR imaging studies (*8*). The resonator has a 4.2-mm-diameter, 10-mm-long, inductive loop, in order to hold a standard 4-mm-od quartz sample tube, and a 10 by 10 mm capacitive gap with 0.46-mm spacing. It can be described as a reentrant LGR. However, the reentrant loops are rectangular, with 10 by 12 and 12 by 12 mm cross sections, to obtain as large a filling factor as possible within the space constraints of the cryostat. The assembly for coupling the resonator to the transmission line, sketched in Fig. 3, is designed to permit both critical coupling for continuous wave (CW) EPR and overcoupling to reduce Q for pulsed EPR. Maximal overcoupling of the resonator occurs when the copper leaf on the end of the center conductor of the transmission line almost touches the conductor that penetrates into the capacitive gap. For each echo experiment, the Q was measured by recording the resonator ring-down after a pulse.

This study used the irradiated fused quartz standard sample (*9*), which is available from Wilmad. This sample is 2 mm in diameter and 10 mm long and was held in a 4-mm-od quartz sample tube (Wilmad) to position it in the resonator. In this resonator, the filling factor for this sample was calculated to be 9.5% by using Ansoft Corporation High Frequency Structure Simulator (HFSS) software to calculate B_1^2 over the sample. This measure of filling factor, relevant to CW EPR, is a useful index of resonator performance.

Microwave pulses were amplified either by a 1-W MiniCir-

FIG. 1. Schematic diagram for 2–4 GHz CW, ESE, and SR microwave bridge. In the following list of components, parameters such as gain and noise figure are given as the minimum and maximum over the 2- to 4-GHz frequency range. When the variation is not large, an approximate average is listed. Numbers are not consecutive because components used in a prior version of the spectrometer were deleted from the final version. (1) Engelmann CC-24 50-mW oscillator; (2) Virtech V31240 isolator; (3), (23), (26), (53), (55), (72) DowKey 401-2208 coaxial switch; (4), (5), (62) Merrimac CSM-30M-3G 30-dB directional coupler; (6), (16) UTE CT-3240-OT isolator; (7) Merrimac PDM-22-3G directional coupler; (8), (20) Arra D4428C phase shifter; (9) Midwest Microwave 1072 0- to 9-dB step attenuator; (10) Midwest Microwave 1071 0- to 60-dB step attenuator; (12), (14), (19), (27), (29), (45), (47) P&H Lab C-1-S26322 isolator; (13), (18), (46) General Microwave DM864BH pin diode switch; (15), (38) Merrimac CSM-10M-3G 10-dB directional coupler; (17) Vectronics DP623.0-67HS 2-bit phase shifter, insertion loss 1.15–2.35 dB, 0, 90, 180, 270° within 4.6°; (22) Arra P4952-80XS phase-constant attentuator; (24) Hughes 8020H 20-W TWT; (25) MiniCircuits ZHL-42 1-W amplifier, 30-dB gain; (28) two M/A Com 2660-9058-00 pin diode switches in series; each has 51.3 dB isolation, 0.9 dB insertion loss, and switches in <27 ns; (31) Virtech VF1556 four-port circulator. 0.8-dB insertion loss; (32) Alpha MT8310A-MF limiter, 0.6-dB insertion loss, 65-mW leakage at 200-W peak, 50 mW at 3-W CW, 15-ns recovery; (34) MITEQ AMF-3B-020040-12 0.9–1.1 amplifier, dB NF, 40.7- to 43.2-dB gain (see also measurement reported in text); (35) MITEQ AMF-4B-2040-7 amplifier, 1.24- to 1.67-dB NF, 27- to 29-dB gain; (36), (69) Dow-Key 435-5208 SP3T coaxial switch; (37), (54) Merrimac CSM-20M-3G 20-dB directional coupler; (39), (40), (61) Virtech VTP2040 crystal detector; (41) Midisco MDC7225 90° hybrid splitter; (42), (43) MiniCircuits ZFM-4212 DBM: (44) Midisco MDC2225 0° power splitter; (48) Western Microwave MN23LX DBM; (49) Arra 4814-20 20-dB adjustable attentuator, 0.5-dB insertion loss; (50) Inmet 8037 DC block; (51) M/A Com MA2696-0101 biphase modulator, 173°, 1.6-dB insertion loss; (52) Virtech V31-2040 isolator; (60) Reactel 4HS 1800S22 highpass filter, >55-dB insertion loss below 1 GHz, <0.5-dB insertion loss above 1 GHz; (63) Midwest Microwave 5011-20 20-dB directional coupler; (64) Midwest Microwave 5011-6 6-dB directional coupler; (65) MiniCircuits ZHL-1042J 25-dB gain amplifier, 4.5-dB NF; (66) 7-dB fixed attenuator; (67) 10-dB fixed attenuator; (70), (71) DowKey 411-2208 coaxial transfer switch; (74) JCA Technology JCA24-F01 22-dB gain amplifier; (75) Microphase CTM324P crystal detector; (76) Advanced Control Components ACLM-4531C limiter. For the 100-KHz amplifier (56), the time domain signal amplifiers (57) and (58), and the 70-KHz amplfier (59), see Figs. 3, 4, and 5 of Ref. (*4*), which also provides a general discussion of the design philosophy and functionality of this type of bridge.

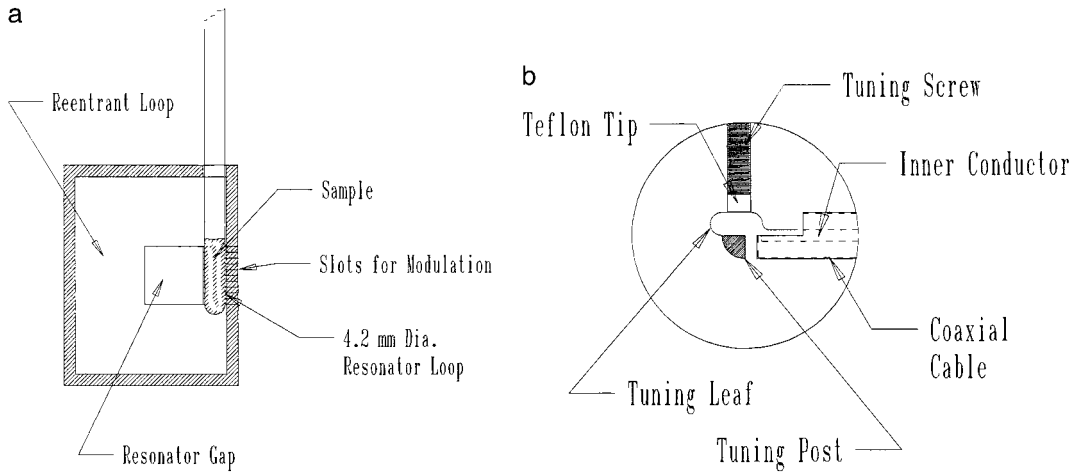

FIG. 3. The resonator used for this study is a loop–gap resonator with a confined return flux path. The region into which the sample is placed is 4.2 mm in diameter and 10 mm long. The capacitive region is 10 by 10 mm, with 0.46-mm spacing. The reentrant lops are rectangular, with 10 by 12 and 12 by 12 mm cross sections, to obtain as large a filling factor as possible within the space constraints of the cryostat in which it was used. Slots cut in the sample region permit penetration of magnetic field modulation for CW EPR. The coupling mechanism, which is adjustable from outside the cryostat, is shown expanded. The tuning screw has 8–80 threads for fine adjustment of the beryllium-copper leaf spring, whose proximity to the inner conductor of the coaxial cable varies the coupling of the resonator to the transmission line. The resonator was made of tellurium copper alloy No. 145 and was not plated. The room temperature critically coupled Q was 460 and it could be overcoupled for pulsed EPR to $Q = 70$.

cuits amplifier (component 25) in the bridge (whose saturated output, measured at the bridge output, is 0.7 W) or by a Hughes 8020H traveling wave tube (TWT) amplifier (component 24), whose saturated output at the frequency used, measured at the output of the bridge, was ca. 8 W. Microwave pulse, phase shifting, and detector protection timing and control were implemented with a locally designed programmable timing unit (*10*). Microwave pulse lengths usually were 40, 80 ns, chosen to ensure that the pulses were minimally affected by the resonator Q. The attenuation of the input to the TWT was adjusted to maximize the echo amplitude. This is approximately the condition for 90°, 180° pulses. Our HFSS calculations show that B_1 in this resonator is uniform within 7% over 8 mm and within 20% over the entire 10-mm length of the sample.

Microwave powers were measured with a Hewlett–Packard 435B power meter, which has a range of 0.3 μW to 3 W with the sensors available. Values on the lowest scale of the HP435B had too large an uncertainty, due to meter drift, to be useful. Calibrated directional couplers and/or low duty cycle were used to measure higher powers.

Echo amplitudes (voltages) were measured by recording the echo with a LeCroy 9310A digital storage oscilloscope (DSO) (LeCroy Corp, Chestnut Ridge, NY), using 50 Ω input, and the noise was measured on the baseline after the echo, using a computational feature of the 9310A, which provides a direct readout of standard deviation.

CHARACTERIZATION OF SPECTROMETER COMPONENTS

To compare calculated and observed signal and noise it is necessary to know the gains and losses, including mismatch, in the path from the resonator to the display. Comparison of locally measured losses for various microwave components with manufacturer specifications revealed that in most cases the manufacturer specifications and factory test results, which usually were reported as “less than,” did not provide the accuracy needed to analyze the spectrometer performance. Consequently, we measured actual losses for sections of the as-built spectrometer and actual gains of the amplifiers. This involved measuring the power input to a portion of the microwave circuit and measuring the power out of that portion of the circuit. The microwave power sources used were the internal source of the bridge or an auxiliary Wavetek Model 962 Micro Sweep (1–4 GHz). The values reported are the average of several measurements made with repeated calibration and zeroing of the HP435B power meter. Gains and losses for various components change with frequency over the octave bandwidth of the bridge. Values reported in this paper are for the specific frequency of 2.68 GHz, at which the echo intensity measurements were made. A summary of the actual gains and losses is presented in Fig. 4 and Table 1. Table 1 compares measurements made on the spectrometer system from resonator to bridge output with the sum of measurements made on individual components and sets of components and presents our judgment of the uncertainties in the measurements. The good agreement provides a firm basis for the calculations of signal and noise presented in this paper.

The DBM was characterized under conditions directly relevant to its use as a detector for the electron spin echo (ESE) signal in the spectrometer. A power meter was used to calibrate the devices and powers used. Power from a microwave source was split and attenuated to provide phase-coherent local oscil-

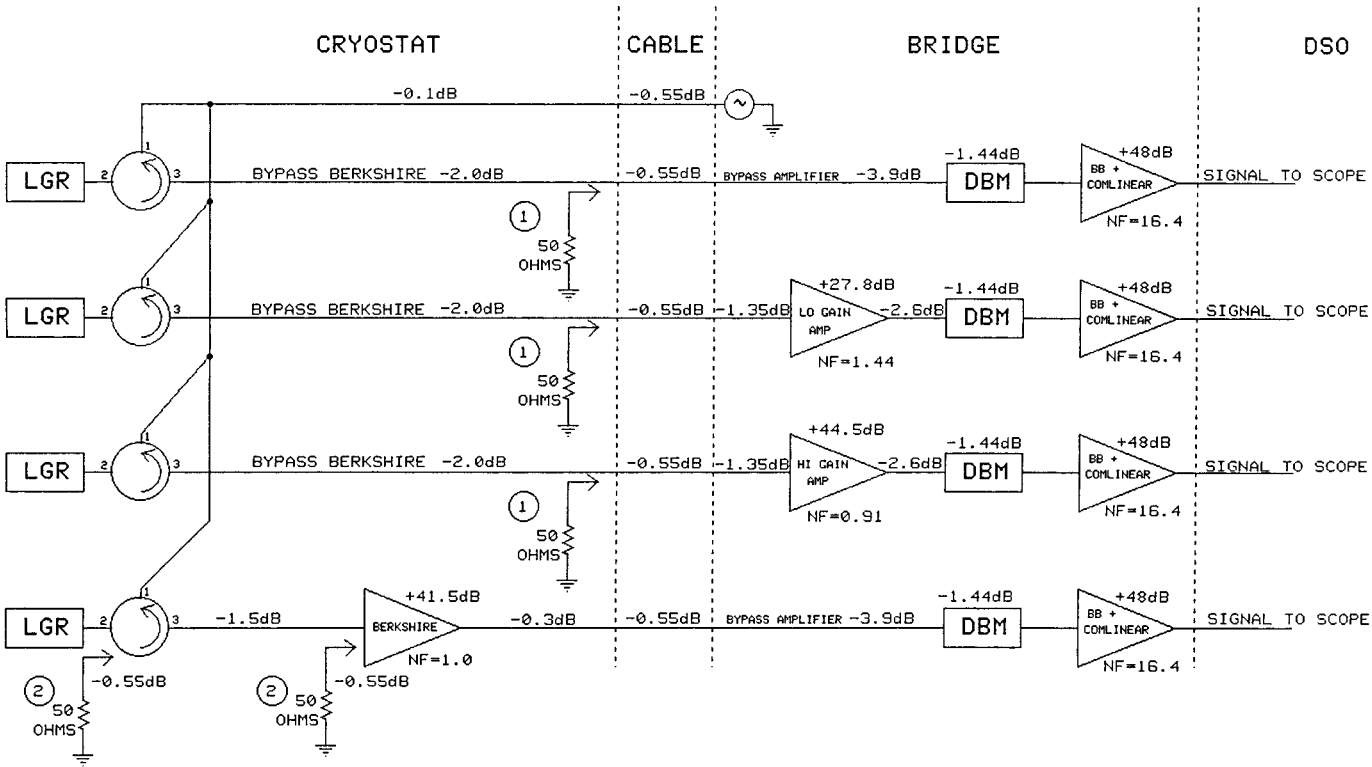

FIG. 4. Schematic signal path with gains and losses noted. The vertical dotted lines separate, from left to right, the cryostat, the cables from the top of the cryostat to the input of the bridge, the bridge, and the cables from the output of the bridge to the signal display system. The collections of components included within each gain or loss block was dictated by measurement convenience. Tests on individual coaxial cables and connectors were too inaccurate to be useful, because the losses were so small, so larger functional units were measured collectively. Gains and losses (negative values) are in dB. Also noted on the diagram are the points at which a 50-Ω load was attached for noise tests reported in Table 2. The 50-Ω load was at the end of a 2-foot flexible coaxial cable (0.55 dB loss), for ease of inserting it in liquid nitrogen. For tests using the amplifiers in the bridge, the 50-Ω load was at the end of the same cable that normally carried signal from the top of the cryostat to the input of the bridge. For the tests of the Berkshire amplifier, the same cable and 50-Ω load were attached at the input to the Berkshire amplifier and for another test at port 2 of the circulator.

lator (LO)-port and RF-port power to the DBM (Western Microwave part No. MN23LX). The LO power was set to a constant 9 mW (+9.5 dBm). The RF-port power first passed through a calibrated attenuator, a TTL-driven biphase modulator, a continuously variable phase shifter, and a calibrated 10-dB coupler to which a power meter was connected for measuring the power input to the RF-port. The X- (or IF-)port output was connected to the 50-Ω input of a LeCroy 9310A oscilloscope. For power calibrations, the biphase modulator was kept in a constant state. For DBM insertion loss measurements, the biphase modulator was driven by a TTL-level 2-KHz square wave (HP 3310A signal generator). This frequency is considerably lower than the high frequency response of the output (X or IF) port of the DBM. The modulation resulted in a square wave response on the scope as the RF phase alternated between 0 and 180°. The output amplitude was measured with various calibrated attenuation settings on the input to the RF-port. The peak-to-peak signal on the scope, divided by 2, eliminated the dc offset inherent in the DBM and yielded the true dc output. For each measurement the RF phase was adjusted to yield the maximum signal on the scope, thereby ensuring that the RF-port phase was the same as the LO-port phase. Four measurements were made, with powers ranging from 8.0 to 14.5 μW input to the RF-port of the DBM,

TABLE 1
Overall Spectrometer System Gain at 2.68 GHz

Path	End-to-end gain (dB)	Voltage gain	Sum of parts (dB)
Berkshire, no loss prior to amplifier	83.4	1.48×10^4	83.3
Berkshire, including loss from resonator to amplifier	81.9 ± 0.2	$1.24 \pm 0.03 \times 10^4$	81.8
No amplifier, from resonator, bypassing Berkshire amplifier	40.1 ± 0.1	101 ± 1	40.1
Low-gain, from resonator bypassing Berkshire amplifier	68.0 ± 0.1	$2.51 \pm 0.003 \times 10^3$	67.9
High-gain, from resonator, bypassing Berkshire amplifier	84.0 ± 0.5	$1.58 \pm 0.09 \times 10^4$	84.6

which are typical powers for ESE signals. Converting the voltage measured into the 50-Ω termination in the LeCroy oscilloscope into power, we find an average mixer loss of −1.44 dB.

The measured conversion loss of −1.44 dB when the DBM was used as a phase detector may seem quite low in light of the manufacturer's specification of 5.5 to 7 dB conversion loss. We could not find a literature reference for this aspect of mixer behavior. However, our insertion loss estimate was verified by a major mixer manufacturer (*11*). The insertion loss for a mixer used as a demodulator (phase-sensitive detector) is quite different than that commonly specified by the manufacturer for a mixer used as a frequency converter. Consequently, we provide a detailed argument here. When the RF and LO frequencies are the same, the DBM functions as a phase-sensitive detector. Since the IF output of the DBM cannot pass the microwave frequencies, it is the average value of the nearly dc output signal that is important. The output changes with time to trace out the amplitude function of the RF input, e.g., the shape of the echo, but it is slowly varying relative to microwave frequencies. The echo and the noise are similarly affected by the electrical properties of the mixer. In an EPR spectrometer, the LO comes from the same source that produces the signal and is, therefore, the same frequency and is adjusted to be in phase with the RF signal in the mixer. The LO is about 9 mW, and the RF signal is in microWatts. Under these conditions the mixer functions essentially as a full-wave (FW) rectifier. The RMS value of a FW-rectified sine wave is the same as the original sine wave, therefore the mixer output power levels are proportional to the power on the RF-port. Except for a small LO to IF leakage, which is specified by the manufacturer as a dc offset in the IF output, none of the power in the detected signal is from the LO. For a peak signal voltage at the RF-port of the DBM of 1 V the RMS value is $1/\sqrt{2}$ and the relative power, which is proportional to $(V_{\mathrm{RMS}})^2$, equals 0.5. The actual power would be 0.5 W for 1-V peak input if the impedance level were 1 Ω. The detected voltage at the IF-port of the DBM is a full-wave rectified sine wave with an ac component at twice the microwave frequency. The bandwidth limitations on the IF response and the amplifiers following the DBM remove the ac component and leave the dc component of the voltage. The dc component of a full-wave rectified sine wave is $2/\pi$ times the peak value. The power level of the detected signal is then $(2/\pi)^2 = 0.405$ W if the impedance were 1 Ω. The apparent insertion loss for a perfectly lossless mixer would then be

$$\text{insertion loss} = 10 \log\left(\frac{0.5}{0.405}\right) = 0.915 \text{ dB}. \qquad [1]$$

This equation will yield the same result regardless of the impedance level, so normalizing to 1-Ω impedance does not affect the result.

This result is consistent with calculating the power level in each harmonic, as was demonstrated by Don Neuf (*11*). The Fourier series for a FW rectified sine wave of amplitude one (1) is

$$\frac{2}{\pi}\left(1 + \tfrac{2}{3}\cos 2\omega t - \tfrac{2}{15}\cos 4\omega t + \tfrac{2}{35}\cos 6\omega t - \cdots\right), \qquad [2]$$

and the relative dc power and power in each harmonic is 0.405, 0.09, 0.003, 0.00066, . . . , respectively. The difference between 0.9 dB and the measured 1.44 dB is attributed to connectors and other nonideal components in the DBM assembly.

The manufacturer specification for a DBM is for its use as a frequency converter, where the input RF signal is converted to two main (sum and difference) frequencies and several harmonic components. In such a case the input RF power is divided between these several frequencies. If the same analysis as outlined above is done for the case when the RF and LO frequencies are not the same, and the LO signal is a large square wave, the theoretical insertion loss from the RF- to the IF-port is 3.92 dB for each of the sum and the difference frequencies (*11*, *12*). The 3.92-dB loss is the 0.915 dB calculated from Eq. [1] plus the 3-dB loss due to dividing the power into two sidebands. The manufacturer specification is for loss greater than the theoretical 3.92-dB loss for IF away from dc, because it is the maximum loss over the specified IF bandwidth (*11*).

EPR SIGNAL INTENSITY

CW EPR signal intensity (voltage) can be written in the form of Eq. [3],

$$V_{\mathrm{S}} = \chi'' \eta Q \sqrt{P_{\mathrm{A}} Z_0}, \qquad [3]$$

where V_{S} is the CW EPR signal voltage at the end of the transmission line connected to the resonator, η (dimensionless) is the resonator filling factor, Q (dimensionless) is the loaded quality factor of the resonator, Z_0 is the characteristic impedance of the transmission line (in Ω), and P_{A} is the microwave power (in W) to the resonator produced by the external microwave source. The magnetic susceptibility of the sample, χ'' (dimensionless), is the imaginary component of the effective RF susceptibility, and for a Lorentzian line with width at half height $= \Delta\omega$ at resonance frequency ω,

$$\chi'' = \chi_0 \frac{\omega}{\Delta\omega}, \qquad [4]$$

where

$$\chi_0 = \frac{N_0 \gamma^2 \hbar^2 S(S+1)\mu_0}{3k_B T}. \quad [5]$$

In this equation the static magnetic field $B_0 = \omega_0/\gamma$, S is the electron spin, k_B is Boltzmann's constant, N_0 is the number of spins per unit volume, T is the temperature of the sample in K. The permeability of vacuum, $\mu_0 = 4\pi \times 10^{-7}\ T^2 J^{-1} m^3$. The spin magnetization is $M_0 = H_0 \chi_0 = B_0/\mu_0\ \chi_0$. Therefore,

$$M_0 = N_0 \frac{\gamma^2 \hbar^2 B_0 S(S+1)}{3k_B T}\ JT^{-1}m^{-3}\ (=Am^{-1}),$$

so M/H is unitless, as required,

and for

$$S = \tfrac{1}{2},\ M_0 = N_0 \frac{\gamma^2 \hbar^2 B_0}{4k_B T}. \quad [6]$$

If resonator size and sample size were kept constant and the noise is determined by the resistive losses in the resonator, then the frequency dependence of each term in Eq. [3] leads to a prediction that S/N varies as $\omega^{7/4}$ in agreement with the analogous arguments put forth by Hoult and Richards (*13*) for certain NMR cases. Since this paper deals with the direct measurement of electron spin echoes, it turns out to be more convenient for calculations to derive the formula for the echo intensity by a different path, as presented in the next section.

CALCULATION OF TWO-PULSE SPIN ECHO INTENSITY

Precessing electron spin magnetization induces a current in the walls of the resonator. The task of calculating the resultant signal level encompasses four major steps. First, the relation between magnetization and signal in the resonator is calculated from first principles, using the inductance and resistance of the resonator. The relation between EPR lineshape and microwave B_1, as described by Bloom (*14*) and Mims (*15, 16*), is used to calculate the echo amplitude. Then the signal in the resonator is transformed to the other side of the resonator coupling device. Gains and losses from this point to the detector are used in the calculation of the predicted echo.

The electron spin echo voltage induced in the resonator is given by

$$V_E = N \frac{d\phi_0}{dt}, \quad [7]$$

where N is the number of turns in the resonator and ϕ_0 is the magnetic flux produced by the spin magnetization, M_0. For all of the work presented here $N = 1$. Since the flux density produced by M_0 is $\mu_0 M_0$, ϕ_0 is given by

$$\phi_0 = \mu_0 \eta \vec{A} \cdot \vec{M}_0, \quad [8]$$

where $\vec{A}$ is the cross sectional area of the coil (resonator sample loop), η is the filling factor, and $\mu_0 = 4\pi 10^{-7}$. M_0 varies sinusoidally at the resonant frequency ω_0, and if the magnetization is fully turned to the xy plane by the microwave pulse, the peak voltage for a single-turn coil (a LGR) is

$$V_E = \mu_0 A \eta \omega_0 M_0 \quad [9]$$

in agreement with (*17*).

The magnetization of the sample was calculated using Eq. [6] based on the spin concentration, N_0, of 3×10^{17} spins/cm^3 ($\pm$10% uncertainty), measured by the technique described in (*9*). The particular quartz sample used in this study has about 60% the spin concentration as the one reported in (*9*). Using tabulated values for the fundamental constants, for this sample ($S = \frac{1}{2}$) $M_0 = 6 \times 10^{-4}\ JT^{-1}m^{-3}$ at 293 K. The sample is a 2-mm-diameter by 10-mm-long cylinder, so the number of spins in the sample is 9.4×10^{15}.

We need to take account of the actual spectrum of the sample relative to the available B_1 at the sample. Calculations of echo shapes were presented by Mims (*15, 16*), who corrected an error in (*14*). In our measurements B_1 was of the same order as, or larger than, the linewidth, and the calculations show that for this case the echo amplitude should approach the maximum possible for the magnetization, M_0. However, this calculation is only part of the story. The Bloom and Mims calculation is for spins on resonance. Off-resonant spins also contribute to the echo (or FID) (*18, 19*), and a $\pi/2$ pulse of strength B_1 will rotate ca. B_1 G of spectrum approximately 90° (*18*). Thus, the Bloom and Mims calculation somewhat underestimates the number of spins observed in an inhomogeneously broadened spectrum. The EPR spectrum of the irradiated quartz sample is only about 2.5 G wide at X band, and most of the spins are within a spectral width of about 0.7 G at S band. Pulse widths, t_p, of 40, 80 ns were used, corresponding to a ca. 4.5-G bandwidth excited by the second (more selective) pulse. The 40-ns $\pi/2$ pulse corresponded to B_1 of ca. 2.2 G. The 3-dB bandwidth of the resonator overcoupled to a Q of 70 was ca. 14 G. Thus, by any of these criteria, the full spectrum was excited. As a further check the echo amplitude was measured for $\pi/2$ pulses of 20 to 100 ns, adjusting the incident power to maximize echo amplitude for each t_p. The echo amplitude was about 20% smaller for the 20, 40 ns pulses, since the Q of the resonator was too high to fully admit the short, rectangular, first pulse, and the second pulse was kept at twice the length of the first pulse. We also performed the very sensitive test for 90° pulses described in (*20*). Our observation of a clean null of the T echo in a $\pi/2{-}\tau{-}\pi/2{-}T{-}\pi/2{-}T{-}$echo

sequence provided further assurance that all of the spins were turned in these measurements. These several approaches to the problem converge on the conclusion that it is reasonable in this case to use M_0 in Eq. [9] to calculate the echo amplitude.

Then, from Eq. [22] of Ref. (*21*), the output voltage of the resonator coupling structure, $V_{E\beta}$, is given by

$$V_{E\beta} = \frac{\sqrt{\beta}}{1+\beta}\sqrt{\frac{Z_0}{R}}\,V_E, \qquad [10]$$

where R is the resistance of the resonator and Z_0 is the impedance of the transmission line (usually 50 Ω). The coupling parameter β is calculated from the overcoupled Q and the critically coupled Q, Q_H, by

$$\beta = \frac{2Q_H}{Q} - 1. \qquad [11]$$

Combining Eqs. [9] and [10] $V_{E\beta}$ can be written as

$$V_{E\beta} = \frac{\sqrt{\beta}}{1+\beta}\sqrt{\frac{Z_0}{R}}\,A\omega_0\eta M_0. \qquad [12]$$

Using the formulae presented in (*22*), the as-built dimensions of the resonator, and the experimental critically coupled $Q = 460$, we calculate $L = 1.46 \times 10^{-9}$ H, and from this $R = 0.027\ \Omega$. Alternatively, we calculate the resistance from the dimensions and the conductivity of copper as 0.027 Ω. This value of R was used in the calculations to convert precessing magnetization to induced voltage.

The concept of filling factor, used in the above derivation, was originated by BPP (*21*), and elaborated by Feher (*24*), Poole (*25*), and Goldberg (*26*) in the context of CW EPR. Abragam (*27*) assumed that inhomogeneous B_1 over the sample could be ignored, and when Hill and Richards (*28*) applied the concept of filling factor to pulsed NMR they carried over the formula from Poole (*25*) and then applied the assumption of uniform B_1 to get the common assumption that the filling factor is the ratio of the volume of the sample to volume of the resonator. The filling factor as described by Poole (*25*) applies in CW EPR (*29*) and is intuitive when one considers the EPR signal as a change in Q due to absorption of power (hence, B_1^2) in the sample. For application to pulsed EPR, we chose not to calculate a filling factor to multiply the magnetization, but instead we calculated directly the echo amplitude as a function of B_1.

The term $\mu_0 M_0 \eta A$ in Eq. [9] represents the magnetic flux that induces a voltage in the resonator:

$$\mu_0 M_0 \eta A = \int_{\text{sample}} \vec{M}\cdot\frac{B_1}{i}\,dV, \qquad [13]$$

where i is the current in the resonator. Thus, the use of the filling factor η is an approximation intended to avoid integrating over the sample. The approximation has to be defined for each case consistent with the experiment.

To calculate the ESE signal voltage directly, substitute [13] into [9],

$$V_E = \omega_0 \int_{\text{sample}} \vec{M}\cdot\frac{B_1}{i}\,dV, \qquad [14]$$

and integrate over the sample volume. Since echo formation is a nonlinear function of B_1 (*14–16*), and B_1 is not uniform over the sample volume, we used the approximation that when B_1 is larger than the spectral width the echo is proportional to $\sin\theta_{pI}\sin^2(\theta_{pII}/2)$, which becomes $\sin^3\theta$ when the second pulse has twice the turning angle, θ, as the first one. Hence, the magnetization in the echo, which is the M to use in [14], is

$$M = M_0 \sin^3\theta, \qquad [15]$$

where θ is calculated from the B_1 generated by HFSS by assuming that at the center of the resonator the turning angle is 90°:

$$\theta = \frac{\pi}{2}\frac{B_{1\perp}}{B_{1\perp,0}} \qquad [16]$$

$B_{1\perp,0}$ is the value of B_1 perpendicular to B_0 at the center of the resonator. We used the HFSS software to calculate the ESE signal. Unfortunately, the HFSS postprocessor has no trig functions, so the following approximation to $\sin\theta$ was used:

$$\sin\theta = \cos\left(\frac{\pi}{2} - \theta\right)$$
$$\cos\theta \approx 1 - 0.4967\theta^2 + 0.03705\theta^4. \qquad [17]$$

This calculation yielded a predicted echo amplitude after the impedance match from the resonator to the transmission line. To compare this prediction with experimental values, we need to know the net signal gain or loss from the resonator to the microwave detector (DBM), and then to the ultimate signal recording device (DSO in this case). The experimental results are sketched in Fig. 4, where the measured signal paths are identified. The net gains for some of the paths are shown in Table 1. In this way we calculated that the peak echo amplitude for the high-gain amplifier path would be 3.0 V at the detector.

The predicted echo amplitude, based on the spin system and the overall system gain, assumes no decay due to relaxation. There is a dead time after the pulses during which one cannot observe the echo, but during which the echo amplitude decays. To account for the decay during the dead time, we measured

the echo decay constant, T_m. The echo decay fits well to a single exponential, since the spin concentration in the sample is high enough that the decay is dominated by instantaneous diffusion (9). Using the experimental T_m of 3 μs, we calculated the echo amplitude at zero time and compared this with the calculated echo amplitude. The measured echo, corrected to zero dead time, was 2.9 V. The agreement is better than the uncertainties in either value.

For comparison we also calculated an approximate function that assumed that all turning angles were 90 and 180°, but that the echo was proportional to the varying B_1. This yielded a 4.2-V echo. If we used Eq. [9] with the Poole η with variations in B_1 over the sample, resulting in $\eta = 0.095$, we calculated a 2.7-V echo. This is also in good agreement with experiment, but the agreement in this case is probably fortuitous.

CALCULATION OF NOISE

Thermal noise generated in the resonator is carried through the same transformations and gains and losses as the signal. In addition, one has to consider noise added from other components. These noise sources can include thermal noise of lossy components, microwave source noise that gets to the detector, microphonics, and pick-up from the environment. In this paper we focus on the electron spin echo measurement, so the microwave source power is off during the time of echo data collection, and there is no magnetic field modulation that might introduce additional noise. Saturation recovery (SR) and CW EPR measurement are more complicated and will be discussed elsewhere.

Thermal noise is caused by the Brownian motion of electrons in a resistor. For our purposes, the available noise power, $p_n(f)$, in W/Hz, is given by (*30*)

$$p_n(f) = k_B T, \qquad [18]$$

where k_B = Boltzmann's constant and T = temperature, K.

Available noise power means the power that will be delivered to a matched load (resistance of load equals resistance of noise source). Often the noise is given in terms of a noise voltage; however, it is more convenient to work with noise power throughout the system and calculate the noise voltage at the detector in terms of the noise power delivered. This should help eliminate the confusion in some texts which often have noise voltage expressions that differ by a factor of 2. The noise power in watts, p_n, is $p_n(f)$ multiplied by the effective noise bandwidth, B, of the system which is often determined by the last stage of the system.

In the development below, we apply the useful concept of noise temperature (*30*). The noise temperature, T_n, of a component is the temperature of a resistive thermal noise source that would produce the same available noise power as the component under consideration. If the component is a thermal source (resistor), the noise temperature is the physical temperature of the component. However, we can calculate the noise temperature for any component even when the source of the noise is not thermal but something else (diode noise, $1/f$ noise, semiconductor shot noise, amplifier noise, etc.). This allows us to use conventional network analysis to calculate the total effective noise temperature for the system and calculate the total contribution to the detected noise voltage, regardless of whether the source of the noise is thermal or not. Below, we determine the expressions for noise temperature for the various components, other than resistors, and for the overall total system noise. First, we need to relate the various noise parameters that are presented in the literature.

The noise figure, NF, of a two-port network is the ratio of the output noise power to the portion of the output noise power that is produced by the input thermal noise source when at standard temperature (290 K). The noise figure can be expressed as a number (ratio) or in dB = $10 \times \log_{10}$(ratio). From this definition it is clear that if the network is noiseless, NF = 1 or 0 dB. Another way to express NF is the ratio, expressed in dB, of the signal-to-noise at the input to the S/N at the output. Thus, if NF = 0 dB, the network is noiseless, since then the S/N at the output is the same as that at the input.

The noise temperature of a component can be calculated from the noise figure. The noise power/Hz at the input due to the thermal noise source at standard temperature, T_0, is $k_B T_0$. The noise power/Hz, also referred to the input of the network, that is added by the network is $k_B T_e$, where T_e is the effective noise temperature of the network (not its physical temperature). The total output noise power/Hz is, then,

$$p_{no}(f) = g(f) k_B (T_0 + T_e) \text{ W/Hz}, \qquad [19]$$

where $g(f)$ is the gain of the network. Now, since the contribution to the output noise power of the thermal source at the input is $g(f) k_B T_0$, the noise figure becomes

$$\text{NF} = 1 + \frac{T_e}{T_0}. \qquad [20]$$

Again it can be seen that if the network is noiseless, $T_e = 0$ and NF = 1. The effective noise temperature in terms of NF is, then,

$$T_e = T_0(\text{NF} - 1). \qquad [21]$$

This equation can be used to determine the noise temperature for any component, such as an amplifier or mixer, when the noise figure is known.

For cascaded networks consisting of n blocks, with the output of each connected to the input of the next, the resulting effective input noise temperature is given by Eq. [22], which is called the Friis equation (*30*).

$$T_{e_{1\ldots n}} = T_{e_1} + \frac{T_{e_2}}{g_1} + \cdots + \frac{T_{e_n}}{g_1 g_2 \cdots g_{n-1}}, \qquad [22]$$

where T_{ei} is the noise temperature of the ith stage, and g_i is the power gain of the ith stage.

It is customary to refer the noise to the input since it eliminates the effect of the gains of each stage. This way, the noise effects of two cascaded networks can be compared directly, the one with the lower noise temperature will have the lowest noise and highest S/N ratio. The effective input noise voltage calculated in this way is presented in Table 4.

The only other relation we need for network components is the noise temperature for an attenuator. In this case the term attenuator includes any element with loss, which in addition to calibrated attenuators, includes resistive losses in transmission lines and mismatch losses in any other components, including connectors and resonators. However, for resistive attenuation, we will assume that the components are critically matched, and mismatch losses will be treated as a separate component. Let the attenuator gain be $g \leq 1$, with source temperature, T_s, and attenuator temperature, T. If the gain is 1 all the noise is due to the input source resistor. If the gain is 0, all of the noise is due to the attenuator. For all other values of gain, the noise is produced in part by the source and in part by the attenuator, and the noise temperature is given by

$$T_e = T\left(\frac{1}{g} - 1\right) \quad 0 < g \leq 1. \qquad [23]$$

Note that when g is 1, $T_e = 0$ since the attenuator adds no noise; however, when g is small T_e becomes quite large. From Eqs. [21] and [23] it can be seen that if the temperature of the attenuator is T_0 then its NF $= 1/g$.

As stated above, Eq. [23] also applies to the resonator, in which case g is the power reflection coefficient (e.g., for 40-dB coupling, $g = 10^{-4}$). It is convenient to refer all noise temperatures to the output of the resonator since this is where the EPR signal originates. The noise temperature for each component before the resonator is then multiplied by its gain and that of all succeeding stages, up to and including the resonator. In this way the contribution of source noise is conveniently included.

Even if a component is at high temperature, if it has no loss, it contributes no noise. This point seems obvious, but we emphasize it here since some researchers have argued informally that a cooled resonator or preamplifier cannot decrease noise if the waveguide between them and the detector is at room temperature. In the predictive model presented below the key entries are the temperature *and* the loss (gain) of each component in the signal path.

We modeled the overall spectrometer S/N behavior using Mathcad 7 (MathSoft, Inc., Cambridge, MA), which facilitates exploring the impact on the final S/N of improving the performance of each component.

TABLE 2
Noise Bandwidth (MHz) of Signal Amplifiers in the Bridge

Nominal amplifier[a] gain	Nominal filter bandwidth (MHz)	Effective noise bandwidth (MHz)
250	No filter	25.7
100	No filter	35.4
250	20	16.8
100	20	17.3
250	5	6.9
100	5	5.5

[a] This amplifier consists of components 57 and 58 in Fig. 1.

MEASUREMENT OF NOISE

The noise figures for the assembly that includes the time-domain signal amplifiers (components 57 and 58, and the filter following 58) were 19.3 dB for a gain of 100 and 16.4 dB for a gain of 250, as calculated from the noise specifications of the devices used in the amplifiers. Since noise measurements depend on the bandwidth of the system, the effective noise bandwidths of the final stage signal amplifier and filter circuits in the bridge were measured (Table 2). These are the amplifier stages presented in Fig. 4 of Ref. (*4*). The output of the amplifier and filter circuit was measured as a function of the input frequency from a swept RF source (Fluke 6082A Synthesized RF Signal Generator, 100 KHz–2112 MHz), and the effective noise bandwidth was computed using Eq. [24] (*30*).

$$NBW = \frac{1}{|H_{max}|^2} \int_0^\infty |H(f)|^2 df, \qquad [24]$$

where $H(f)$ is the output of the filter divided by the input, and H_{max} is the maximum value of $H(f)$.

When the 50-Ω load (1 or 2 in Fig. 4) was cooled in liquid nitrogen (77 K), the measured standard deviation noise decreased. Similar tests were performed using the Berkshire amplifier, the low-gain amplifier, and the "no amplifier" path in the bridge. The 50-Ω load was placed in two locations to test the effect of the room-temperature circulator: in one test the flexible cable with the 50-Ω load at the end was attached directly to the input of the Berkshire amplifier; in the other test the cable and load were attached to port 2 of the circulator, where the signal from the resonator normally enters. Also in Table 4 are noise measurements made under similar conditions, except that the signal path from the resonator was connected to the bridge. All of these measurements were made under pulsed EPR conditions, with the PIN diode switches

being turned on and off. The measured standard deviation noise varied only 1–2 mV for various attenuations of the output of the 1-W internal amplifier or the 20-W TWT amplifier. The uncertainty in the noise measurements is ca. ± 1 mV for the high-gain MITEQ and Berkshire amplifiers and less than 1 mV for the other two paths.

To test the noise produced in the bridge itself, a 50-Ω load was put at the end of a 24-inch (1 inch = 2.54 cm) flexible cable on the input to the bridge, in place of the signal from the resonator. When the noise was measured with no filtering following the DBM other than the inherent filtering of the components, we observed the values in Table 4. The measured output standard deviation noise voltages were divided by the measured overall system voltage gain to obtain the equivalent measured input noise voltages tabulated. For example, with the LGR at 294 K and using the high-gain MITEQ amplifier the actual measured output standard deviation noise was 80 mV. Dividing by the gain yields an equivalent input noise of 4.7 μV. The calculated value for this case was 4 μV. The equivalent input noise voltages give an indication of relative S/N, since the gain affects noise and signal in the same way.

COMPARISON OF MEASURED AND PREDICTED NOISE

From Table 4 it can be seen that the calculated values compare very well with the measured values when no microwave amplifier is used. This indicates that the parameters for the DBM and the gain and noise bandwidth of the amplifier after the DBM are accurate. The calculated and measured values do not agree as well for the paths that include one of the low-noise microwave preamplifiers, with discrepancies as large as 20%. However, the ratio of the measured and calculated noise voltages for 294 and 77 K agree to within a few percent. This agreement indicates that the measured noise voltage is primarily thermal noise, and the discrepancy between the calculated and measured noise voltages is most likely due to inaccuracy in the overall voltage gain estimates. We are not aware that this level of quality of spectrometer performance has previously been demonstrated. The observation that overall spectrometer system noise performance is well described by the model presented above validates this model for future spectrometer system design.

Reviewers of this paper and other colleagues have inquired about whether the small discrepancies between calculated and observed noise in this study could be due to what is sometimes called "excess noise." Experimental noise due to thermal effects (*31–33*) on conductors (now known as Johnson noise) agrees with predictions based on thermodynamics and statistical mechanics for most conductors (*34*, *35*), and the agreement extends to the microwave region (*36*). The statistical conditions are different for devices such as thermionic tubes and photoelectric cells and for other devices not obeying Ohm's law (*34*). The documented exceptions to the predictions of Johnson noise involve resistors which are granular in nature, such as composite carbon resistors and sputtered metal films (*31*). The physical picture presented (*31*) involves a fluctuating resistance at the points of contact between granules. The type of resistor used as a load in the study reported in this paper is a metal film resistor (verified by the manufacturer) which has a noise temperature essentially equal to its physical temperature.

Another possible question concerns the effect a change in resistance will have when the load is cooled. We consider two possible effects. One is that the noise from the load will decrease as the temperature is lowered due to the Boltzmann distribution. The second effect is that the resistance might change and thereby affect the matching. If only the matching changes the noise will not change. This is because the noise power attenuated by the mismatch is made up for by the loss associated with the mismatch. Any change in the source noise due to the Boltzmann distribution will be propagated to the following stages in the circuit. Furthermore, the 50-Ω load used in the tests was measured on a Hewlett–Packard Network analyzer at temperatures from 77 to 290 K. The reflection coefficient was essentially constant over that range of temperatures.

Finally, the equations used, and in particular Eq. [22], fully account for mismatch (see (*30*), particularly Chapter 8) and the effect of mismatch on noise.

COMPARISON OF PREDICTED AND OBSERVED SIGNAL AND NOISE

Using the gains appropriate to the "high-gain" MITEQ amplifier and gain = 250 for the amplifier that follows the DBM, we calculated 3.0-V echo and observed 2.9-V echo. These values agree within the uncertainty in each of them. We observed single-shot $S/N = 30$ to 50. The calculated echo signal at the resonator was 190 μV, and the observed equivalent input noise voltages at 294 K were ca. 3–4 μV, in good agreement with the experimental S/N.

The measured noise is close to that predicted based on the properties of the components in the bridge, with the input to the bridge being the thermal noise from a 50-Ω load. (Note that 1 dB = 12% in voltage.) These conditions approximate the case common in most spectrometers, where there are lossy elements at room temperature even if the sample is cooled to cryogenic temperatures. The question to be answered is whether a low-noise amplifier, even a cooled amplifier, is of any value in such a case. Both the measurements and the calculations show that for room temperature operation even a low-gain (27.8 dB) low-noise (NF = 1.44) amplifier improves S/N by a factor of 7 to 8 relative to no microwave preamplifier, because of the high noise figure of the subsequent stages in an EPR bridge (16.4 dB, see Fig. 4). When all components before the low-noise amplifier are at 77 K, the improvement in S/N is 9 to 10. Our model indicates that improving the noise figure of the amplifier in the bridge to NF = 0 dB (i.e., a perfect amplifier that adds no noise) would decrease

the calculated output noise from 66.8 mV to 60.2 mV for the high-gain amplifier and from 11.1 mV to 9.6 mV for the low-gain amplifier. Since the output EPR signal would remain the same, this improvement in noise figure would result in an improvement in S/N by 10 and 13.5%, respectively. Thus, there is a measurable advantage with an improved microwave preamplifier in the room-temperature bridge, but as will be discussed below, greater advantage accrues from placing the amplifier closer to the sample and cooling it.

The calculated values in Table 2 are based on the gains and losses listed in Table 1 and Fig. 4, with all noise being due to thermal noise in the lossy elements and the noise added by the amplifiers used. The measured noise is always higher than the calculated noise. Should the excess of measured noise over calculated noise be attributed to noisy electronic environment of the bridge? Such attribution is made implausible by the close agreement (within 3% worst case) with calculation of the noise reduction upon cooling the 50-Ω load. Nevertheless, we need to consider possible reasons for the discrepancies. The higher the gain of the amplifier, the larger the discrepancy between the calculated and measured value. The disagreement is larger than our best estimates of the uncertainties in the measured gains and losses. Considering the versatility built into the bridge, with many alternate pathways for both source microwave energy and signal, and the fact that there are two power amplifiers in close proximity to the low-noise signal amplifiers, a "sneak" path which contributes an additional noise source not included in the model is possible. Placement of microwave absorber material near the low-noise microwave preamplifiers prior to the measurements reported here did decrease the noise, especially low-frequency noise, measured under some conditions in CW, and especially superheterodyne, EPR. A single-purpose bridge, optimized to decrease the loss between the resonator and the amplifier, would also minimize the number of connectors through which additional microwave power could leak and presumably would give lower noise performance than the bridge described here. However, were there an additional contribution of noise in the bridge, it would not explain the excess noise observed with the Berkshire amplifier, which is physically remote from the bridge. An alternative explanation for the higher than calculated noise would be that the gains of the amplifiers are higher than we measured them to be, or the noise figures are higher than the manufacturers reported them to be. Although we cannot resolve these matters to better than the 20% (maximum) discrepancy, a crucial observation is that cooling of the 50-Ω load to 77 K resulted in a decrease in noise, in agreement with the model. As pointed out above, these measurements demonstrate that the dominant noise in this spectrometer is thermal noise.

HOW TO IMPROVE SPECTROMETER *S/N* PERFORMANCE

Any loss between the resonator and the first stage amplification proportionately decreases the S/N. Hence, the flexibility built into the spectrometer described here is a direct tradeoff with S/N performance. To optimally implement any of the special experiments designed into this spectrometer as switched paths, a special-purpose path should be built in which the signal does not undergo the losses of the switched paths. For example, for CW operation better S/N would be obtained by removing the limiter, which contributes most of the loss prior to the amplifier in the present system. Based on the model presented, one can predict that placing the Berkshire amplifier immediately on the output of the resonator instead of sending the signal through the circulator and limiter, should increase the S/N by ca. 1.5 dB (19%). The only practical way to put an amplifier at this location would be to use a cross-loop resonator (*5, 6*); however, we consider the alternate location of the amplifier to illustrate the effect of various losses in the system. If the Berkshire amplifier were replaced with a perfect amplifier (NF = 0 dB) directly on the output of the resonator, the S/N would improve by 2.4 dB (32%).

When the first amplifier is the amplifier in the bridge, there is 3.9-dB signal loss prior to the amplifier. If the amplifier were directly on the output of the resonator the signal would increase by a factor of 1.6. This loss is reduced from 3.9 to 1.5 dB by using the Berkshire amplifier in the present configuration (Fig. 4a). The Berkshire amplifier has about 3 dB lower gain than the high-gain MITEQ amplifier in the bridge and about the same noise figure, at 2.77 GHz. Accounting for actual performance as best we can estimate it, we predict an improvement of S/N of about 33% when the Berkshire amplifier is used relative to when the high-gain MITEQ amplifier is used, and for single echoes we observe $S/N = 51$ and 36 (echo extrapolated to time zero), respectively, an improvement of 42%.

For perspective on S/N improvements, note that over the full history of commercial EPR spectrometers, the improvement in S/N attributable to bridge and console electronics (as opposed to resonator improvements) has been linear in time, from ca. 60 in the late 1960s to ca. 360 in the latest Bruker spectrometers. This comparison is for CW spectra of the standard weak pitch sample in a TE_{102} rectangular cavity resonator. See (*37*) for a discussion of the use of the pitch standard and changes in the measurement over time.

Standard CW EPR spectrometers inherently have higher noise than the ESE spectrometer described here, because in a CW spectrometer microwave source power is on during EPR signal observation. Some source power is reflected from the resonator due to imperfect match, and power leaks through the circulator due to imperfect isolation, adding source noise to the EPR signal.

Not discussed in this paper are improvements in S/N that can result from optimization of the resonator to the spectroscopic problem. For example, when thermal noise from the resonator dominates, S/N is proportional to ηQ, so it will increase linearly with the filling factor, η, if the resonator Q does not decrease due to the proportionately larger sample. Similarly, the Q should be as high as is consistent with the maximum permissible dead time for time-domain experiments,

as discussed in (*21*). For nonlossy, unlimited samples dramatic improvements in CW S/N are achievable with high-Q resonators, if the source noise does not dominate. As has been shown for ESE (*21*), it is always better to overcouple a high-Q resonator than to use an inherently low-Q resonator to decrease dead time.

COMPARISON OF PULSED AND CW EPR SIGNAL INTENSITIES

The ratio of CW EPR signal intensity to electron spin echo intensity for the same sample is the ratio of Eq. [3] to Eq. [12]. For clarity, set $\beta = 1$, which is always experimentally possible if the relaxation time is long enough. The algebra simplifies if it is noted that one can use the substitutions $Q_L = \omega L/2R$, $L = \mu_0 A/l$, where l is the length of the loop–gap resonator, and $\sqrt{P}/(l\sqrt{R}) = H_1$, with which it can be shown that

$$\frac{\text{CW}}{\text{Echo}} = \frac{\gamma B_1}{\Delta\omega} = \frac{B_1}{\Delta B}. \qquad [25]$$

For convenience, we have written the ratio in both frequency and field units. This ratio implies that if the echo is formed by all of the spins in the sample (see Eq. [12]), the unsaturated CW spectral intensity is equal to the microwave B_1 divided by the EPR linewidth, times the echo intensity. Most commercial EPR spectrometers have an output microwave power of 200 mW. For a standard rectangular resonator (loaded $Q \approx 3600$), this corresponds to a B_1 at the sample of ca. 0.5 G. If the EPR line is about 2.5 G wide, which could be fully excited by a microwave pulse, then the unsaturated CW EPR intensity at 200 mW would be ca. 0.2 times the intensity of the echo. In practice, most CW spectra are obtained with magnetic field modulation. If the magnetic field modulation were approximately equal to the linewidth, this ratio would still hold. Such a large magnetic field modulation would distort the signal, so in practice a smaller modulation amplitude is usually used, resulting in a proportionately smaller CW signal relative to the echo signal.

The presentation of noise in terms of equivalent input noise voltage (Table 4) helps one compare thermal noise voltage and signal voltage values (the signal is essentially RMS, so the numbers are directly comparable) at the resonator (see Table 3). For the quartz sample used in these experiments we calculated an echo signal at the resonator of 190 μV. The comparable thermal noise voltage is 2.2 μV in a 50-Ω load if there is 25.7-MHz bandwidth (noise power available is $-174 + 10$ log(bandwidth) dBm). Another way of saying this is that if all of the active devices had NF = 0 dB, the equivalent input noise voltage would be 2.2 μV, so a 190-μV signal would have $S/N = 86$, and a 2.2-μV signal would be detectable with $S/N = 1$. The sample contained ca. 9.4×10^{15} spins (based on the sample size and concentration, as given above). The extrapolated ultimate sensitivity then is ca. 1.1×10^{14} spins with $S/N = 1$ if the only noise is thermal noise. The number of spins detectable with S/N = 1 decreases if the bandwidth is narrower, since the noise is proportional to the square root of the bandwidth. One way to narrow the effective bandwidth is to signal average (*38*), in which case the effective noise bandwidth decreases with the square root of the number of scans averaged. Thus, it is not totally artificial to consider a pulse experiment with a 1-Hz bandwidth due to signal averaging, and we consider the hypothetical case in which the ESE detection system has a 1-Hz bandwidth in order to make a rough comparison with CW EPR sensitivity specifications. The thermal noise voltage in a 50-Ω load at 290 K detected with a 1-Hz bandwidth would be 4.5×10^{-10} V, and one could observe 2.2×10^{10} spins with $S/N = 1$ and other parameters kept constant.

TABLE 3
Measured and Calculated Echo Amplitudes

Amplifier path	Observed echo, corrected to time = 0	Calculated echo
No amplifier	ca. 0.019	0.019
Low-gain	0.43	0.48
High-gain	2.9	3.0
Berkshire	2.2	2.4

COMPARISON WITH X-BAND SENSITIVITY

It is well-known that state-of-the-art X-band EPR spectrometers are stated to have a CW sensitivity ($S/N = 1$) equivalent to 0.8×10^{10} spins/G at 200 mW for a nonsaturable, nonlossy sample, extending through a TE_{102} cavity, assuming an $S = \frac{1}{2}$ system with a single Lorentzian line, with 1-s time constant and optimum magnetic field modulation. Note that the standard commercial definition of noise for sensitivity tests is peak-to-peak divided by 2.5, whereas the standard deviation noise we use is more nearly equal to peak-to-peak divided by 5, but in some conventions various numbers of noise spikes are ignored. To compare the number of spins required for $S/N = 1$ in the S-band spin echo experiment with the current CW S/N specifications for commercial X-band spectrometers it is necessary to consider differences in ηQ, spectrometer frequency, and detection system bandwidth. Our best estimates of the Q and filling factor are that the ηQ product is roughly twice as large for the quartz sample in the S-band resonator as in an X-band TE_{102} cavity. However, if the same number of spins as in the 10-mm-long sample were extended along the entire length of the X-band cavity, analogous to the weak pitch sample used in sensitivity tests, the signal would be about a factor of 2 weaker (0.39 for a line vs a point sample, accounting for the nonuniform distribution of B_1 and modulation amplitude, and 0.5 if the modulation were uniform, according to Ref. (*39*)). Thus, to

TABLE 4
Equivalent Input Noise Voltage[a] (μV)

Amplifier path	Voltage gain	50-Ω load, 294 K Calculated	50-Ω load, 294 K Measured	50-Ω load, 77 K Calculated	50-Ω load, 77 K Measured	Voltage gain	LGR, 294 K, $\beta = 12$ Calculated	LGR, 294 K, $\beta = 12$ Measured
No amplifier	127.5	30.25	29.8	30.18	29.8	101.3	38	37.5
Low-gain	3112	3.55	4.1	2.97	3.4	2472	4.5	5.3
High-gain	21,280	3.14	3.76	2.47	2.9	16900	4.0	4.7
Berkshire						12320	3	3.5
Berkshire, 50-Ω load on circulator input	11,560	3.2	3.9	2.6	3.1			
Berkshire, 50-Ω load on amplifier input	13,740	2.7	3.2	1.9	2.2			

[a] Equivalent input noise is the observed output noise divided by the gain of the measured part of the system. Note that the end-to-end voltage gain (Table 1) is slightly different from the gain estimated from the sum of parts (Fig. 4 and Table 1) due to roundoff and uncertainties in gains and losses of individual components. The values in Fig. 4 were used in the Friis equation to calculate the equivalent input noise voltage in this table.

within our ability to estimate relevant parameters, the Q, η, and modulation distribution factors approximately cancel. Using a critically coupled resonator for the X-band CW measurement instead of an overcoupled resonator (as used for the S-band echo measurement) would result in a factor of ca. 2 stronger signal at X band (*21*). The frequency difference per se would result in a factor of ca. $3.4^{7/4}$ stronger signal at X band, other things being equal (*40, 41*). The ratio of CW to echo intensities, calculated above, was ca. 0.2, so the net effect will be that the X-band CW signal will be roughly $2 \times 3.4^{7/4} \times 0.2 = 3.4$ times the S-band echo signal. Within the accuracy of these estimates we would predict a sensitivity of 6.5×10^9 spins/G at X band if all of the spins contribute to a 1-G Lorentzian line. Since errors from approximations could tend to accumulate, we estimate the sensitivity by a different path, starting with 0.8×10^{10} spins/G, and then using Eq. [3] for V_S with best estimates of η (ca. 1%) and Q (ca. 3600) we calculate an X-band signal voltage of ca. 6×10^{-10} V prior to amplification. This compares with the noise voltage of 4.5×10^{-10} V in a 1-Hz bandwidth, yielding S/N slightly greater than 1 within the accuracy of the estimates.

The actual noise in the S-band measurement is slightly higher than the thermal noise used in these estimates because of the noise added (Eq. [22]) between the resonator and the final recorded signal. Similarly, the CW X-band EPR S/N specification is for a spectrometer for which noise is greater than the thermal limit. Current X-band CW spectrometers probably have noise contributions from microphonics (including that due to use of high modulation amplitude), source noise (especially at high microwave power), and detector preamplifier noise (most spectrometers do not use a low-noise microwave preamplifier). However, current commercial X-band CW spectrometers are within small factors of the best S/N we can estimate by these methods. The standard weak pitch S/N measurement is performed with magnetic field modulation larger than the linewidth to maximize the signal amplitude (although distorting the lineshape) and thus approximates the assumptions used in our treatment of the CW signal. Thus, both the CW and the echo experiments measure approximately the total signal voltage. Note that in a field-modulated CW measurement in which the lineshape is to be preserved, the modulation amplitude should be less than about 1/10 of the linewidth, so the signal voltage is substantially reduced from the maximum possible.

A key message from this example is that sensitivity (S/N) differences between CW and pulsed EPR are a strong function of detector bandwidth and modulation amplitude.

The primary task in applying the approach presented in this paper to other spectrometers is measurement of the properties of the resonator and of the components in the signal path.

CONCLUSIONS

The validity of the model is shown by the agreement with experiments for the echo signal and noise for the four signal paths compared. The primary conclusion is that the extremely-low-noise (by historical standards) microwave amplifiers now available significantly improve S/N compared with signal paths without a microwave preamplifier. In addition, there is a distinct advantage to having the microwave amplifier as close to the sample as possible. In addition, if the amplifier is coolable, its noise figure should decrease with a decrease in temperature. The calculations also show that having this microwave amplifier cooled, especially when the resonator and sample are cooled, will yield the best S/N.

Absolute echo amplitudes and absolute noise can be calculated to within the accuracy with which the properties of the resonator and the gains and losses of the microwave components in the signal path can be measured. The calculational and experimental approach applied here to a specific S-band ESE

spectrometer can be applied to guide attainment of the ultimate possible S/N for other pulsed EPR spectrometers.

ACKNOWLEDGMENTS

This research was supported in part by NSF Grant BIR-9316827 (GRE) and NIH Grant GM57577 (GAR). This paper benefited from two very thorough critical reviewers whose detailed comments and questions caused us to add substantial additional discussion of several aspects of mixers and of noise that are not well-described in the literature. Reference *12* was brought to our attention by a reviewer.

REFERENCES

1. J. S. Hyde "Experimental Techniques in EPR," 6th Annual NMR–EPR Workshop, Nov. 5–9, 1962, Varian Associates Instrument Division, Palo Alto, CA, as cited by Alger (1968).
2. R. S. Alger, "Electron Paramagnetic Resonance: Techniques and Applications," pp. 200 ff, Wiley–Interscience, New York, (1968).
3. S. Pfenninger, W. Froncisz, and J. S. Hyde, Noise analysis of EPR spectrometers with cryogenic microwave preamplifiers, *J. Magn. Reson. A* **113,** 32–39 (1995).
4. R. W. Quine, G. A. Rinard, B. T. Ghim, S. S. Eaton, and G. R. Eaton, A 1–2 GHz pulsed and continuous wave electron paramagnetic resonance spectrometer, *Rev. Sci. Instrum.* **67,** 2514–2527 (1996).
5. G. A. Rinard, R. W. Quine, B. T. Ghim, S. S. Eaton, and G. R. Eaton, Easily tunable crossed-loop (bimodal) EPR resonator, *J. Magn. Reson. A* **122,** 50–57 (1996).
6. G. A. Rinard, R. W. Quine, B. T. Ghim, S. S. Eaton, and G. R. Eaton, Dispersion and superheterodyne EPR using a bimodal resonator, *J. Magn. Reson. A* **122,** 58–63 (1996).
7. J. S. Hyde and W. Froncisz, The loop-gap resonator: A new microwave lumped circuit ESR sample structure. *J. Magn. Reson.* **47,** 515–521 (1982).
8. A. Sotgiu and G. Gualtieri, Cavity resonator for in vivo ESR spectroscopy, *J. Phys. E. Sci. Instrum.* **18,** 899–901 (1985).
9. S. S. Eaton and G. R. Eaton, Irradiated fused quartz standard sample for time domain EPR, *J. Magn. Reson. A* **102,** 354–356 (1993).
10. R. W. Quine, Programmable timing unit for generating multiple coherent timing signals. U.S. Patent No. 5,621,705, issued April 15, 1997 and No. 5,901,116 issued May 4, 1999.
11. Don Neuf, Special Mixer Products Department, Miteq, Inc., 100 Davids Drive, Hauppauge, NY, private communication, December 17, 1998.
12. A. J. Kelly, Fundamental limits on conversion loss of double sideband resistive mixers, *IEEE Trans. Microwave Theory Techniques* **MTT-25,** 867–869 (1977).
13. D. I. Hoult and R. E. Richards, The signal-to-noise ratio of the nuclear magnetic resonance experiment, *J. Magn. Reson.* **24,** 71–85 (1976).
14. A. L. Bloom, Nuclear induction in inhomogeneous fields, *Phys. Rev.* **98,** 1105–1111 (1955).
15. W. B. Mims, Electron echo methods in spin resonance spectrometry, *Rev. Sci. Instrum.* **36,** 1472–1479 (1965).
16. W. B. Mims, Electron spin echoes, *in* "Electron Paramagnetic Resonance" (S. Geschwind, Ed.), Plenum Press, New York (1972).
17. N. Bloembergen and R. V. Pound, Radiation damping in magnetic resonance experiments, *Phys. Rev.* **95,** 8–12 (1954).
18. J. P. Hornak and J. H. Freed, Spectral rotation in pulsed ESR spectroscopy, *J. Magn. Reson.* **67,** 501–518 (1986).
19. E. Fukushima and S. B. W. Roeder, "Experimental Pulse NMR. A Nuts and Bolts Approach," section II.A.2, Addison–Wesley, Reading, MA (1981).
20. W. H. Perman, M. A. Bernstein, and J. C. Sandstrom, A method for correctly setting the rf flip angle, *Magn. Reson. Med.* **9,** 16–24 (1989).
21. G. A. Rinard, R. W. Quine, S. S. Eaton, G. R. Eaton, and W. Froncisz, Relative benefits of overcoupled resonators vs. inherently low-Q resonators for pulsed magnetic resonance, *J. Magn. Reson. A* **108,** 71–81 (1994).
22. G. A. Rinard, R. W. Quine, S. S. Eaton, and G. R. Eaton, Microwave coupling structures for spectroscopy, *J. Magn. Reson. A* **105,** 134–144 (1993).
23. N. Bloembergen, E. M. Purcell, and R. V. Pound, Relaxation effects in nuclear magnetic resonance absorption, *Phys. Rev.* **73,** 679–712 (1948).
24. G. Feher, Sensitivity considerations in microwave paramagnetic resonance absorption techniques. *Bell System Technical J.* **36,** 449–484 (1957).
25. C. P. Poole, Jr., "Electron Spin Resonance: A Comprehensive Treatise on Experimental Techniques," p. 524, Wiley–Interscience, New York (1967).
26. I. B. Goldberg and H. R. Crowe, Effect of cavity loading on analytical electron spin resonance spectrometry, *Anal. Chem.* **49,** 1353–1357 (1977).
27. A. Abragam, "The Principles of Nuclear Magnetism," p. 74, Oxford Univ. Press, London, (1961).
28. H. D. W. Hill and R. E. Richards, Limits of measurement in magnetic resonance. *J. Phys. E. 2* **1,** 977–983 (1968).
29. M. Sueki, G. A. Rinard, S. S. Eaton, and G. R. Eaton, Impact of high dielectric loss materials on the microwave field in EPR experiments, *J. Magn. Reson. A* **118,** 173–188 (1996).
30. "Transmission Systems for Communications." Revised 4th ed., Bell Telephone Laboratories, Western Electric Company, Inc., Technical Publications, Winston–Salem, North Carolina, 1971, pp. 170–171 and Chaps. 7 and 8.
31. C. J. Christensen and G. L. Pearson, Spontaneous resistance fluctuations in carbon microphones and other granular resistances. *Bell System Technical J.* **15,** 197–223 (1936).
32. Radio Engineering Handbook (K. Henney, Ed.), pp. 2-13–2-14, McGraw–Hill, New York (1959).
33. R. Morrison, "Noise and Other Interfering Signals," pp. 77–78, Wiley, New York (1991).
34. J. B. Johnson, Thermal agitation of electricity in conductors, *Phys. Rev.* **32,** 97–109 (1928).
35. H. Nyquist, Thermal agitation of electrical charge in conductors, *Phys. Rev.* **32,** 110–113 (1928).
36. R. H. Dicke, The measurement of thermal radiation at microwave frequencies, *Rev. Sci. Instrum.* **17,** 268–275 (1946).
37. S. S. Eaton and G. R. Eaton, Quality assurance in EPR, *Bull. Magn. Reson.* **13,** 83–89 (1992).
38. T. H. Wilmshurst, "Signal Recovery from Noise in Electronic Instrumentation," 2nd ed., p. 87, Hilger–IOP Publishing, Bristol (1990).
39. Varian Publication 87-125-502, E231 multipurpose cavity.
40. G. R. Eaton, S. S. Eaton, and G. A. Rinard, Frequency dependence of EPR sensitivity, *in* "Spatially Resolved Magnetic Resonance" (P. Blümler, B. Blümich, R. Botto, and E. Fukushima, Eds.), pp. 65–74, Wiley–VCH Publ., Weinheim (1998).
41. G. A. Rinard, R. W. Quine, R. Song, J. Harbridge, G. R. Eaton, and S. S. Eaton, Frequency dependence of EPR signal to noise. *J. Magn. Reson.,* in press (1999).